

Plasmon enhanced near-infrared quantum cutting and simulation analysis of β -NaYF₄:Tb³⁺, Yb³⁺ doped with Ag nanoparticles

BIAO ZHENG,¹ LIN LIN,^{1,2,3,4} ZHUOHONG FENG,^{1,2,3} ZHIPENG YU,¹ ZHEZHE WANG,^{1,2,3} SENYUAN XU,¹ AND ZHIQIANG ZHENG^{1,2,3,*}

¹College of Physics and Energy, Fujian Normal University, Fuzhou 350117, China

²Fujian Provincial Key Laboratory of Quantum Manipulation and New Energy Materials, Fuzhou 350117, China

³Fujian Provincial Collaborative Innovation Center for Optoelectronic Semiconductors and Efficient Devices, Xiamen 361005, China

⁴llin@fjnu.edu.cn

*zqzheng@fjnu.edu.cn

Abstract: Nanoscale quantum cutting (QC) phosphor β -NaYF₄:Tb³⁺,Yb³⁺ nanoparticles (NPs) and noble metal Ag NPs are synthesized respectively, then β -NaYF₄:Tb³⁺,Yb³⁺ NPs are doped with Ag NPs uniformly. Experimentally, plasmon enhanced near-infrared (NIR) QC involving a Yb³⁺ ion at 977nm (²F_{5/2}→²F_{7/2}) emission is achieved under 377nm (⁷F₆→⁵D₃) excitation of Tb³⁺ ions. The QC luminescence intensity first increases, then decreases with the increase of Ag NPs concentration. The maximum QC luminescence enhancement factor reaches 2.4 when the concentration of Ag NPs is 0.25%. Theoretically, a 3D finite-difference time-domain (FDTD) simulation is carried out to numerically estimate the electric field enhancement around Ag NPs, and then the theoretical QC luminescence enhancement factor is calculated. Our study may provide a promising QC layer on the top of silicon-based solar cells to improve the photovoltaic conversion efficiency.

© 2016 Optical Society of America

OCIS codes: (240.6680) Surface plasmons; (160.5690) Rare-earth-doped materials; (250.5230) Photoluminescence; (260.2160) Energy transfer; (160.4236) Nanomaterials.

References and links

1. B. M. van der Ende, L. Aarts, and A. Meijerink, "Near-Infrared Quantum Cutting for Photovoltaics," *Adv. Mater.* **21**(30), 3073–3077 (2009).
2. X. Chen, S. Li, G. J. Salamo, Y. Li, L. He, G. Yang, Y. Gao, and Q. Liu, "Sensitized intense near-infrared downconversion quantum cutting three-photon luminescence phenomena of the Tm³⁺ ion activator in Tm³⁺Bi³⁺:YNbO₄ powder phosphor," *Opt. Express* **23**(3), A51–A61 (2015).
3. A. Guille, A. Pereira, C. Martinet, and B. Moine, "Quantum cutting in CaYAlO₄: Pr³⁺, Yb³⁺," *Opt. Lett.* **37**(12), 2280–2282 (2012).
4. K. Deng, T. Gong, L. Hu, X. Wei, Y. Chen, and M. Yin, "Efficient near-infrared quantum cutting in NaYF₄: Ho³⁺, Yb³⁺ for solar photovoltaics," *Opt. Express* **19**(3), 1749–1754 (2011).
5. Z. Liu, N. Dai, and J. Li, "High-efficient near-infrared quantum cutting based on broadband absorption in Eu²⁺-Yb³⁺ co-doped glass for photovoltaic applications," *Appl. Phys. A-Mater* **119**(2), 553–557 (2015).
6. B. Zheng, S. Xu, L. Lin, Z. Wang, Z. Feng, and Z. Zheng, "Plasmon enhanced near-infrared quantum cutting of KYF₄: Tb³⁺, Yb³⁺ doped with Ag nanoparticles," *Opt. Lett.* **40**(11), 2630–2633 (2015).
7. W. Zhu, D. Chen, L. Lei, J. Xu, and Y. Wang, "An active-core/active-shell structure with enhanced quantum-cutting luminescence in Pr-Yb co-doped monodisperse nanoparticles," *Nanoscale* **6**(18), 10500–10504 (2014).
8. L. Lin, H. Lin, Z. Wang, J. Chen, R. Huang, Z. Feng, and Z. Zheng, "Quantum-cutting of KYF₄:Tb³⁺,Yb³⁺ under multiple excitations with high Tb³⁺ concentration," *Opt. Mater.* **36**(6), 1065–1069 (2014).
9. Y.-T. An, C. Labbé, J. Cardin, M. Morales, and F. Gourbilleau, "Highly Efficient Infrared Quantum Cutting in Tb³⁺-Yb³⁺ Codoped Silicon Oxynitride for Solar Cell Applications," *Adv. Opt. Mater.* **1**(11), 855–862 (2013).
10. Z. Liu, J. Li, L. Yang, Q. Chen, Y. Chu, and N. Dai, "Efficient near-infrared quantum cutting in Ce³⁺-Yb³⁺ codoped glass for solar photovoltaic," *Sol. Energy. Mat. Sol. C.* **122**, 46–50 (2014).
11. T. Trupke, M. A. Green, and P. Würfel, "Improving solar cell efficiencies by down-conversion of high-energy photons," *J. Appl. Phys.* **92**(3), 1668–1674 (2002).

12. Y. Qin, Z. Dong, D. Zhou, Y. Yang, X. Xu, and J. Qiu, "Modification on populating paths of β - $\text{NaYF}_4:\text{Nd}/\text{Yb}/\text{Ho}@/\text{SiO}_2@/\text{Ag}$ core/double-shell nanocomposites with plasmon enhanced upconversion emission," *Opt. Mater. Express* **6**(6), 1942 (2016).
13. P. Yuan, Y. H. Lee, M. K. Gnanasammandhan, Z. Guan, Y. Zhang, and Q.-H. Xu, "Plasmon enhanced upconversion luminescence of $\text{NaYF}_4:\text{Yb},\text{Er}@/\text{SiO}_2@/\text{Ag}$ core-shell nanocomposites for cell imaging," *Nanoscale* **4**(16), 5132–5137 (2012).
14. X. Chen, W. Xu, L. Zhang, X. Bai, S. Cui, D. Zhou, Z. Yin, H. Song, and D. H. Kim, "Large Upconversion Enhancement in the "Islands" $\text{Au}-\text{Ag}$ Alloy/ $\text{NaYF}_4:\text{Yb}^{3+},\text{Tm}^{3+}/\text{Er}^{3+}$ Composite Films, and Fingerprint Identification," *Adv. Funct. Mater.* **25**(34), 5462–5471 (2015).
15. N. S. Abadeer, M. R. Brennan, W. L. Wilson, and C. J. Murphy, "Distance and Plasmon Wavelength Dependent Fluorescence of Molecules Bound to Silica-Coated Gold Nanorods," *ACS Nano* **8**(8), 8392–8406 (2014).
16. E. He, H. Zheng, J. Dong, W. Gao, Q. Han, J. Li, L. Hui, Y. Lu, and H. Tian, "Facile fabrication and upconversion luminescence enhancement of $\text{LaF}_3:\text{Yb}^{3+}/\text{Ln}^{3+}@/\text{SiO}_2$ ($\text{Ln} = \text{Er}, \text{Tm}$) nanostructures decorated with Ag nanoparticles," *Nanotechnology* **25**(4), 045603 (2014).
17. Z. Li, L. Wang, Z. Wang, X. Liu, and Y. Xiong, "Modification of $\text{NaYF}_4:\text{Yb},\text{Er}@/\text{SiO}_2$ nanoparticles with gold nanocrystals for tunable green-to-red upconversion emissions," *J. Phys. Chem. C* **115**(8), 3291–3296 (2011).
18. Y.-L. Wang, N. M. Estakhri, A. Johnson, H.-Y. Li, Z. Zhang, A. Alù, and C.-K. K. Shih, "Tailoring Plasmonic Enhanced Upconversion in Single $\text{NaYF}_4:\text{Yb}^{3+}/\text{Er}^{3+}$ Nanocrystals," *Sci. Rep.* **5**, 10196 (2015).
19. T. Ming, H. Chen, R. Jiang, Q. Li, and J. Wang, "Plasmon-controlled fluorescence: beyond the intensity enhancement," *J. Phys. Chem. Lett.* **3**(2), 191–202 (2012).
20. C. Lorbeer, J. Cybinska, and A. V. Mudring, "Facile preparation of quantum cutting $\text{GdF}_3:\text{Eu}^{3+}$ nanoparticles from ionic liquids," *Chem. Commun. (Camb.)* **46**(4), 571–573 (2010).
21. Y. Sun and Y. Xia, "Shape-controlled synthesis of gold and silver nanoparticles," *Science* **298**(5601), 2176–2179 (2002).
22. J. Cao, L. Chen, W. Chen, D. Xu, X. Sun, and H. Guo, "Enhanced emissions in self-crystallized oxyfluoride scintillating glass ceramics containing KTb_2F_7 nanocrystals," *Opt. Mater. Express* **6**(7), 2201 (2016).
23. M. Fujii, T. Nakano, K. Imakita, and S. Hayashi, "Upconversion luminescence of Er and Yb codoped NaYF_4 nanoparticles with metal shells," *J. Phys. Chem. C* **117**(2), 1113–1120 (2013).
24. P. K. Jain and M. A. El-Sayed, "Plasmonic coupling in noble metal nanostructures," *Chem. Phys. Lett.* **487**(4-6), 153–164 (2010).

1. Introduction

The increasing demand for solar energy, due to energy crisis and environmental pollution of fossil-fuel, has put how to improve the photovoltaic conversion efficiency of solar cells at the forefront of research [1]. The mismatch between the solar spectrum and the band gap energy of silicon semiconductor limits the photovoltaic conversion efficiency of silicon-based solar cells, because photons with energy lower than the band gap cannot be absorbed, while for photons with energy larger than the band gap, the excess energy is lost by thermalization of hot charge carriers [2]. In order to make full use of the solar energy, there have been increasing efforts on improving the conversion efficiency of silicon-based solar cells, and one of them is quantum cutting (QC) [3–8]. The QC process can convert one ultraviolet-visible (UV-Vis) solar photon (300–500nm) into two near-infrared (NIR) photons (~1000nm), which can be efficiently absorbed by silicon-based solar cells [9, 10]. Therefore, the solar spectrum modulation through QC process can improve the photovoltaic conversion efficiency in the silicon-based solar cells [11].

Recently, noble metal nanoparticles (NPs) have been applied to enhance the upconversion luminescence of rare-earth (RE) ions doped phosphors [12–15]. This is because that the incorporation of noble metal NPs can enhance the luminescence of RE ions when the excitation or emission wavelength of RE ions is near the surface plasmon resonance (SPR) wavelength of noble metal NPs [16, 17]. The mechanism of this plasmon enhanced upconversion luminescence of RE ions is called as local field enhancement effect (LFE) [18]. However, there is little report on plasmon enhanced QC luminescence of QC phosphors doped with noble metal NPs [6]. Furthermore, on one hand, most of QC phosphors are synthesized by sol-gel method or solid state reaction. These phosphors have a large and nonuniform particle size, usually in micron size, which will scatter and waste the incident light [8]. On the other hand, only a lower QC luminescence enhancement factor can be expected in these phosphors, because the area of local electric field surrounding Ag NPs mostly exists within 30nm from the surface of Ag NPs [19], as shown in Fig. 1. These

problems will limit the potential application of QC phosphors as a QC layer. To overcome these problems, the QC nano-phosphor with small and uniform sized should be adopted, which will minimize the scattering of the incident light and improve the plasmon enhanced QC luminescence efficiency [20]. In this paper, nanoscale $\beta\text{-NaYF}_4\text{:Tb}^{3+}$, Yb^{3+} NPs are synthesized, then $\beta\text{-NaYF}_4\text{:Tb}^{3+}$, Yb^{3+} NPs are doped with Ag NPs uniformly. Experimentally, an efficient plasmon enhanced NIR QC luminescence is achieved in $\beta\text{-NaYF}_4\text{:Tb}^{3+}$, Yb^{3+} NPs doped with Ag NPs. Theoretically, the 3D finite-difference time-domain (FDTD) simulation is carried out to numerically estimate the electric field enhancement around Ag NPs, and then the theoretical NIR QC luminescence enhancement factor is calculated to explain the experimental results. Our study will provide a better candidate for application as QC layer on the top of silicon-based solar cells to improve the photovoltaic conversion efficiency.

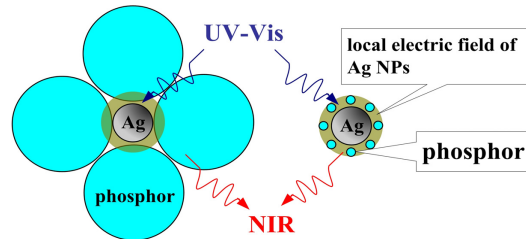


Fig. 1. Mechanism of plasmon enhanced NIR QC luminescence by Ag NPs.

2. Experimental

The hexagonal fluoride $\beta\text{-NaYF}_4$ NPs was chosen as QC host due to its low phonon frequencies and high chemical and thermal stability [13]. 2mmol $\beta\text{-NaYF}_4\text{:15%Tb}^{3+}$, 10% Yb^{3+} NPs were synthesized through coprecipitation method, which were introduced thoroughly in the literature [7]. The silver solutions (1ml containing 1.5625×10^{-5} mol Ag NPs) were prepared by chemical reduction method [21], in which Ag^+ was reduced to Ag by ethylene glycol (EG) in the presence of poly (vinylpyrrolidone) (PVP) and a trace amount of Na_2S . Next, the $\beta\text{-NaYF}_4$ NPs were doped with the Ag NPs homogeneously by a facile method as following: a proper amount of as-synthesized $\beta\text{-NaYF}_4\text{:15%Tb}^{3+}$, 10% Yb^{3+} NPs and silver solution were mixed uniformly, ultrasonic oscillated for 1h, and dried out in a agate mortar at 60°C for 8h, yielding the $\beta\text{-NaYF}_4\text{:Tb}^{3+}$, Yb^{3+} NPs doped with Ag NPs, as shown in the schematic illustration at Fig. 2. In order to research the optimal doped concentration of Ag NPs in the QC luminescence process, a series of $\beta\text{-NaYF}_4\text{:15%Tb}^{3+}$, 10% Yb^{3+} NPs doped with $x\%$ Ag NPs ($x = 0, 0.1, 0.2, 0.25, 0.3, 0.35, 0.5, 0.6$) (Tb/Yb/Ag with mole ratio) was prepared. The amount of $\beta\text{-NaYF}_4$ NPs was 2mmol (0.4136g). The volume of silver solutions was $128\mu\text{l}$ (0.1% Ag), $256\mu\text{l}$ (0.2% Ag), $320\mu\text{l}$ (0.25% Ag), $384\mu\text{l}$ (0.3% Ag), $448\mu\text{l}$ (0.35% Ag), $640\mu\text{l}$ (0.5% Ag), and $768\mu\text{l}$ (0.6% Ag), respectively.

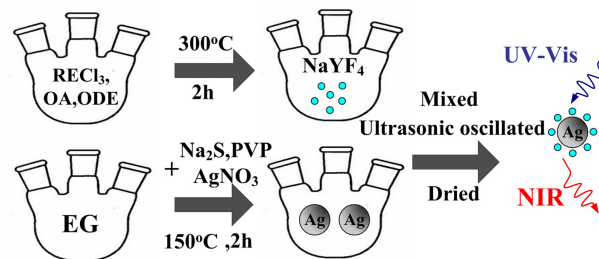


Fig. 2. Schematic illustration of the synthesis of $\beta\text{-NaYF}_4$ NPs doped with Ag NPs.

As-prepared samples were characterized by X-ray diffraction (XRD, MiniFlex II, Rigaku), fluorescence spectra (Fluorolog 3-22 spectrofluorometer, Horiba Jobin Yvon),

scanning electron microscope (SEM) attached with energy dispersive X-ray analysis (SU8010, Hitachi), and absorption spectra (Lambda 950, PerkinElmer).

A 3D FDTD simulation of Ag NPs was performed by FDTD Solutions 8.15, which was developed by Lumerical Solutions, Inc. During the FDTD simulation, an electromagnetic pulse with a central wavelength of 377nm was launched into a box containing an Ag NP. The Ag NP and its surrounding space were divided into 0.5nm meshes.

3. Results and discussion

The UV-Vis absorption spectrum and the corresponding morphology of Ag NPs solution are shown in Fig. 3(a). There is a broad absorption band from 320nm to 700nm, peaked at 420nm, which indicates that the SPR wavelength of Ag NPs is around 320nm to 700nm. The inset of Fig. 3(a) shows that the size distribution of Ag NPs is from 100nm to 150nm.

Figure 3(b) illustrates the XRD pattern of β -NaYF₄:Tb³⁺,Yb³⁺ NPs. All major diffraction peaks match well with those of β -NaYF₄ phase (JCPDS 16-0334). The XRD results indicate that the sample is well crystallized and doped RE ions can substitute Y³⁺ ions without disturbing the crystal lattice. The corresponding SEM image of β -NaYF₄:Tb³⁺,Yb³⁺ NPs is presented in Fig. 3(c). It can be observed that the β -NaYF₄:Tb³⁺,Yb³⁺ NPs are well-dispersed and uniform with an average diameter of about 20nm.

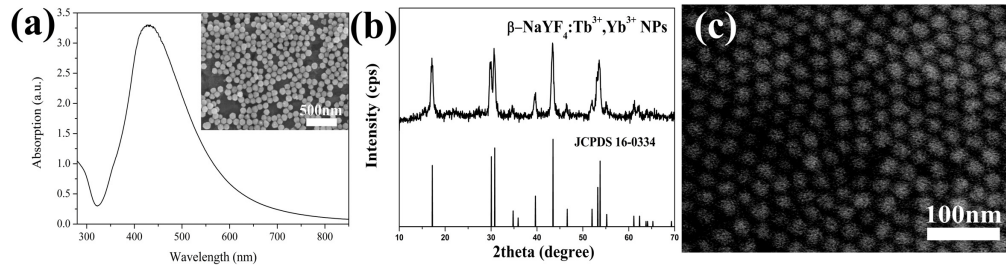


Fig. 3. (a) UV-Vis absorption spectrum of Ag NPs solution. Inset: Corresponding SEM image of Ag NPs solution. (b) XRD patterns of the β -NaYF₄:15%Tb³⁺, 10%Yb³⁺ NPs. (c) Corresponding SEM image of the β -NaYF₄:15%Tb³⁺, 10%Yb³⁺ NPs.

To observe the distribution of Ag NPs in β -NaYF₄:Tb³⁺,Yb³⁺ NPs, the SEM image of β -NaYF₄:Tb³⁺,Yb³⁺ NPs doped with Ag NPs is measured. According to Fig. 4 (a), Ag NPs are surrounded by β -NaYF₄:Tb³⁺,Yb³⁺ NPs uniformly and the Ag NPs doesn't cluster. To further confirm that β -NaYF₄:Tb³⁺,Yb³⁺ NPs are doped with Ag NPs homogeneously, the images of X-ray surface scanning analysis of β -NaYF₄:Tb³⁺,Yb³⁺ NPs doped with Ag NPs are measured in Fig. 4(b). The distributions of Ag, Tb, Yb elements are homogenous in the sample, which can further demonstrate that β -NaYF₄:Tb³⁺,Yb³⁺ NPs are doped with Ag NPs homogeneously.

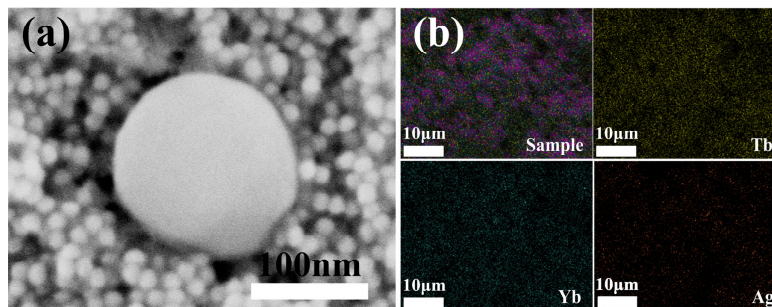


Fig. 4. (a) SEM image of β -NaYF₄:15%Tb³⁺, 10%Yb³⁺ NPs doped with 0.5%Ag NPs. (b) Images of X-ray surface scanning analysis of β -NaYF₄:15%Tb³⁺, 10%Yb³⁺ NPs doped with 0.5%Ag NPs.

To research the influence of Ag NPs on the NIR QC luminescence in β -NaYF₄:Tb³⁺,Yb³⁺ NPs, the excitation spectra monitored at 977nm and emission spectra excited at 377nm of β -NaYF₄:Tb³⁺,Yb³⁺ NPs doped with different Ag concentrations are measured, respectively. From the excitation spectra in Fig. 5(a), the major excitation peaks are located at 350nm, 368nm, 377nm, and 487nm, attributed to $^7F_6 \rightarrow ^5D_2$, $^5L_{10}$, 5D_3 , 5D_4 transitions of Tb³⁺ ions, respectively [22]. The excitation intensity increases with increasing Ag NPs concentration from 0% to 0.25%. Then, it decreases with further increase of Ag NPs concentration, which mainly ascribes to the stronger extinction on the incident light due to the larger concentration of Ag NPs [15]. The maximum excitation enhancement factor is about 2.5.

Figure 5(b) demonstrates the NIR emission spectra of β -NaYF₄:Tb³⁺,Yb³⁺ NPs doped with different Ag concentrations under 377nm excitation. From the NIR emission spectra, the major emission peak is located at 977nm, attributed to the $^2F_{5/2} \rightarrow ^2F_{7/2}$ transitions of Yb³⁺ ions. The emission intensity increases with increasing Ag NPs concentration from 0% to 0.25%, and then decreases with the further increase of Ag NPs concentration, which indicates that plasmon enhanced QC luminescence is achieved. The maximum QC luminescence enhancement factor is about 2.4 excited at 377nm. The details of this plasmon enhancement mechanism will be discussed in the next paragraph. In addition, the possibility that energy transfer from Ag NPs to Yb³⁺ ions can be excluded, because the SPR peak (320nm to 720nm) of Ag NPs isn't observed in the excitation spectra monitored at 977nm (See Fig. 5(a)).

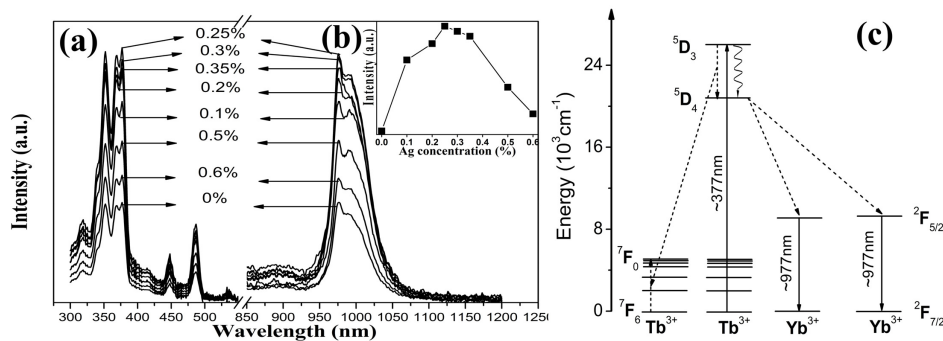


Fig. 5. (a) Excitation spectra ($\lambda_{em} = 977\text{nm}$) and (b) NIR emission spectra ($\lambda_{ex} = 377\text{nm}$) of β -NaYF₄:15%Tb³⁺, 10%Yb³⁺ NPs doped with $x\%$ Ag NPs ($x = 0, 0.1, 0.2, 0.25, 0.3, 0.35, 0.5, 0.6$). Inset: NIR emission intensity vs. Ag concentration. (c) Energy levels diagram of Tb³⁺, Yb³⁺ ions in the NIR QC energy transfer.

Figure 5(c) illustrates the NIR QC mechanism of Tb³⁺, Yb³⁺ ions in terms of the energy level diagrams. Initially, the Tb³⁺ ions are pumped from the ground level 7F_6 to an excited level 5D_3 under 377nm excitation. Then, the 5D_3 level of Tb³⁺ ions relaxes to 5D_4 level by the cross-relaxation ($^5D_3 + ^7F_6 \rightarrow ^5D_4 + ^7F_0$) and nonradiative transition ($^5D_3 \rightarrow ^5D_4$). The cooperative energy transfer occurs from one Tb³⁺ ion in excited level 5D_4 to two neighbor Yb³⁺ ions in the ground level. That is, two Yb³⁺ ions are pumped to the excited level $^7F_{5/2}$ via a coupled transition $^5D_4 \rightarrow ^7F_6$ of one Tb³⁺ ion. Finally, the NIR QC luminescence at 977nm is emitted from the transition ($^7F_{5/2} \rightarrow ^7F_{7/2}$) of the excited Yb³⁺ ions. In our case, the incorporation of Ag NPs in β -NaYF₄ NPs will enhance the excitation rate of Tb³⁺ ions attributed to the local field enhancement effect of Ag NPs, because the excitation wavelength (377nm) is near the SPR wavelength (320nm-700nm) of Ag NPs. Subsequently, the emission of Yb³⁺ ions at 977nm is also enhanced through cooperative energy transfer from Tb³⁺ ions to Yb³⁺ ions. In this way, the plasmon enhanced NIR QC luminescence is achieved.

To calculate the theoretical QC luminescence enhancement of β -NaYF₄:Tb³⁺, Yb³⁺ NPs doped with Ag NPs, the electric field enhancement of the Ag NPs is numerically estimated through 3D FDTD simulation. As reported in the literatures [23, 24], the theoretical QC luminescence enhancement factor caused by LFE of Ag NPs can be expressed as

$$Y = |L(\omega_{ex})|^2 Z(\omega_{em})$$

Where $L(\omega_{ex})$ is the excitation enhancement factor of the incident electric field by the excitation of localized surface plasmon, $Z(\omega_{em})$ is the emission enhancement factor due to the enhancement of the radiative rate. Because the emission peak (977nm) of Yb^{3+} ions is far from the SPR wavelength of Ag NPs, the emission enhancement factor is considered as 1. Therefore, the theoretical QC luminescence enhancement factor can be re-written as $Y = |L(\omega_{ex})|^2$.

The 3D FDTD simulation is carried out to numerically estimate the electric field distribution around Ag NP. As shown in Fig. 6, the Ag NP is considered as a sphere of 100nm in diameter. Since the distance between two neighboring Ag NPs is much larger than the diameter of Ag NP, the influence of other Ag NPs is negligible. The simulation results show that the Ag NP generates the localized surface plasmons and substantial electric field enhancement around the Ag NP. The incident electric field enhancement factor $L(\omega_{ex})$ with a average value of 2 is reached close to the surface of the Ag NP, and decreases with the increase of distance from Ag NP surface. As a consequence, the theoretical QC luminescence enhancement factor $|L(\omega_{ex})|^2$ with a average value of 4 is reached close to the surface of Ag NP, and decreases with the increase of distance from Ag NP surface. Considering the Ag NPs are surrounded by plenty of $\beta\text{-NaYF}_4$ NPs (See Fig. 4 (a)), it is reasonable that the experimental QC luminescence enhancement factor (~ 2.4) is smaller than the theoretical QC luminescence enhancement factor (~ 4).

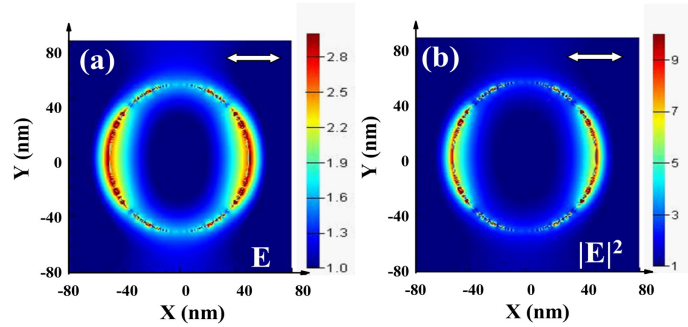


Fig. 6. Contours of simulated electric field enhancement (a) $L(\omega_{ex})$ and (b) $|L(\omega_{ex})|^2$ around one Ag NP excited at 377nm.

4. Conclusions

Nanoscale QC phosphor $\beta\text{-NaYF}_4\text{:Tb}^{3+}$, Yb^{3+} NPs are synthesized by coprecipitation method and noble metal Ag NPs are synthesized by chemical reduction method, respectively. Then, $\beta\text{-NaYF}_4\text{:Tb}^{3+}$, Yb^{3+} NPs are doped with Ag NPs uniformly. Experimentally, plasmon enhanced NIR QC involving Yb^{3+} ions at 977nm emission is achieved under 377nm excitation of Tb^{3+} ions. The effect of Ag NPs on NIR QC luminescence is investigated, and the results show that QC luminescence intensity first increases, then decreases with the further increase of the Ag NPs concentration. The maximum QC luminescence enhancement factor reaches 2.4 when the concentration of Ag NPs is 0.25%. Theoretically, the 3D FDTD simulation is carried out to numerically estimate the electric field enhancement around Ag NPs, and then the theoretical QC luminescence enhancement factor is calculated. Our study may provide a promising QC layer on the top of silicon-based solar cells to improve the photovoltaic conversion efficiency.

Funding

National Natural Science Foundation of China (NFSC) (11204039, 51202033); Natural Science Foundation of Fujian Province of China (2015J01243, 2016J01213); Science Foundation of the Educational Department of Fujian Province of China (JA13084).